In situ stress evolution of Co films sputtered onto oxidized Si (100) substrates

M. Pletea,[a] W. Brückner, H. Wendrock, and R. Kaltofen
Leibniz-Institut für Festkörper und Werkstoffforschung, Helmholtzstraße 20, D-01069 Dresden, Germany

R. Koch
Paul-Drude-Institut für Festkörperelektronik, Hausvogteiplatz 5-7, D-10117 Berlin, Germany

(Received 22 August 2005; accepted 14 December 2005; published online 7 February 2006)

The stress of magnetron-sputtered Co films of thicknesses up to 300 nm has been investigated in a wide range of sputter pressures (0.05-6 Pa) by a laser-based optical bending-beam setup. To correlate the thickness dependence of the stress with changes in the microstructure, the film morphology was investigated by focused ion beam, scanning electron microscopy, and atomic force microscopy. At all of the chosen sputter pressures the film stress is tensile. At low sputter pressures its evolution with film thickness can be related to the Volmer-Weber growth mode of medium-mobility metals and is similar to that of sputtered Cu films concerning nuclei density, island size, and island growth. At higher sputter pressures a transition to columnar grain growth takes place, accompanied by a decrease of the film density and an increase of the electrical resistance. The evolution of stress and microstructure with film thickness is discussed in the context of the stress models proposed in the literature. © *2006 American Institute of Physics*. [DOI: 10.1063/1.2168243]

I. INTRODUCTION

Cobalt single layers and Co-based multilayers are of considerable interest for applications in ultralarge-scale integrated circuits, information storage media, and magnetoresistive devices.[1–3] Therefore, knowledge and control of the stress development in Co films is an important issue for device functionality and reliability as well as for an understanding of the basic physical properties[4,5] (e.g., the stress-induced anisotropy is often mentioned as one of the origins of the perpendicular magnetic anisotropy[6]).

Systematic *in situ* stress measurements[7–9] performed during evaporation of various films revealed that, depending on the adatom mobility, the stress behavior of polycrystalline films can be grouped into two categories. In low-melting-point metals (i.e., high adatom mobility) such as Cu, Ag, and Al, the stress changes from compressive to tensile to compressive with increasing film thickness (type I). High-melting-point metals (i.e., low adatom mobility) such as Co, Ni, Cr, Fe, and W develop only tensile stress irrespective of the film thickness (type II). The specific stress behavior is correlated with different growth modes of the films.[10]

Only few *in situ* stress measurements of evaporated[11–13] and sputtered[14] Co films have been reported. Stress studies by Thornton *et al.*[15] carried out on sputtered films of the two types mentioned above led to the following conclusions: (i) With increasing sputter pressure the intrinsic stress passes a tensile stress maximum and decreases again. At low sputter pressures the stress can also become compressive. (ii) The critical pressure at which the transition from tensile to compressive stress takes place decreases with the decreasing atomic mass of the sputtered material.

In this paper we present the results of *in situ* stress measurements during and after the sputter deposition of Co films onto thermal-oxidized Si (100) substrates at various sputter pressures. In order to correlate the stress evolution to changes in the morphology, the microstructure of the Co films was investigated by focused-ion-beam (FIB) microscopy, scanning electron microscopy (SEM), atomic force microscopy (AFM), and electron backscatter diffraction (EBSD). The stress evolution is compared with that of Cu films[16] investigated recently and discussed with respect to the stress models proposed in the literature. Our work is part of a research project focusing on the *in situ* stress evolution during sputter deposition of Co and Cu single layers and Co/Cu multilayers.

II. EXPERIMENTAL PROCEDURE

The stress measurements were performed in a planar dc magnetron sputter system that allows the deposition of single layers as well as multilayers. A bending-beam device based on laser-optical detection of the substrate deflection has been used to study the stress evolution in real time. The details concerning construction and operation of the experimental setup can be found elsewhere.[16] The substrate deflection is proportional to the force per unit width F/w, which is equal to the product between the average stress $<\sigma>$ and the film thickness t_f. It is calculated according to the well-known Stoney equation[17] from the change in the position of the two laser beams on the detectors Δ_1 and Δ_2 by

$$\frac{F}{w} = \langle\sigma\rangle t_f = -\frac{1}{12}\frac{E_s}{1-\nu_s}\frac{t_s^2}{d_b L}(\Delta_2 - \Delta_1). \quad (1)$$

$E_s/(1-\nu_s)$ and t_s denote the biaxial modulus and thickness of the substrate, respectively $[E_s/(1-\nu_s) = 180.5$ GPa

[a]Electronic mail: t.m.pletea@ifw-dresden.de

 © 2006 American Institute of Physics

Downloaded 09 Feb 2006 to 193.174.238.119. Redistribution subject to AIP license or copyright, see http://jap.aip.org/jap/copyright.jsp

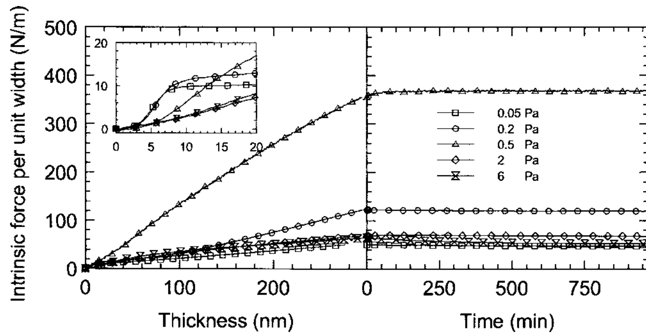

FIG. 1. Evolution of the intrinsic force per unit width measured continuously during (left) and after (right) the sputter deposition of Co films with a rate of 0.05 nm/s and at various Ar pressures as indicated. The thermal force component has been subtracted from the experimental data. The inset shows the evolution of $(F/w)_{int}$ during the early stages of deposition.

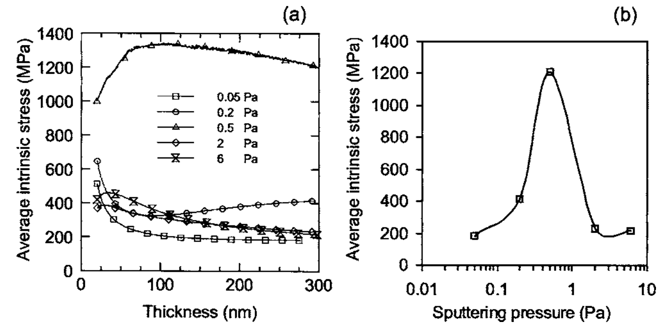

FIG. 2. The evolution of the average intrinsic stress during the sputter deposition of Co films calculated from Fig. 1 for film thickness above 10 nm (a) and the average intrinsic stress at 300 nm as a function of Ar pressure (b). The thermal stress component has been subtracted from the experimental data.

and $t_s=375$ μm], and d_b and L are the distance between the two parallel beams and the substrate-detector optical path, respectively ($d_b=30$ mm and $L=495$ mm).

The base pressure of the sputter system was 10^{-6} Pa. The cobalt target with a purity of 99.99% had a diameter of 75 mm. The mean distance between the target and the grounded substrate was of 175 mm. Argon with a purity of 99.998% was introduced as a working gas into the deposition chamber with a mass flow rate of 10 SCCM (SCCM denotes cubic centimeter per minute at standard temperature and pressure). The sputter pressure was varied in the range of 0.05-6 Pa. In order to keep a constant deposition rate of 0.05 nm/s, the discharge power was varied between 30 and 300 W depending on the sputter pressure used. The film thickness was controlled continuously during the deposition by means of a quartz-crystal oscillator and was checked after the deposition by a Dektak stylus profiler. The substrate temperature was determined by a thermocouple during and after the deposition.

The microstructure analyses of the sputtered films were performed *ex situ* with a focused ion beam system FIB 200 (FEI Company), a field-emission SEM (FE-SEM) Gemini 1530 (Zeiss NTS) equipped with an EBSD system Channel 5 (HKL Technology), as well as a Veeco DI 3100 AFM.

The electrical resistance of the Co films was measured at room temperature (RT) by the van der Pauw method. In order to estimate the mass density of the samples the weight was measured before and after the deposition.

III. RESULTS

Figure 1 shows the evolution of the intrinsic component of the force per unit width $(F/w)_{int}$, which develops during and after the sputter deposition of 300-nm-thick Co films at RT and various sputter pressures. $(F/w)_{int}$ is obtained by subtracting the thermal stress contribution from the measured F/w curve. During the deposition the substrate temperature increases slightly by 4° to 15° depending on the Ar pressure. The corresponding thermal stress is calculated by using the linear thermal-expansion coefficients of the substrate and thin film at RT (i.e., $\alpha_{Si}=2.5\times10^{-6}$ K^{-1} and $\alpha_{Co}=12.5\times10^{-6}$ K^{-1}) and the biaxial modulus of the thin film (i.e., $E_f=211$ GPa and $\nu_f=0.32$ for polycrystalline Co). The thermal component $(F/w)_{th}$ is compressive and estimated to be smaller than 23% of the measured F/w. For example, at a sputter pressure of 6 Pa a value of $(F/w)_{th}=15$ N/m is obtained for a 300-nm-thick Co film.

At all film thicknesses and sputter pressures $(F/w)_{int}$ is tensile (Fig. 1). At low Ar pressures (0.05 and 0.2 Pa) a relatively large tensile stress contribution is observed at the early stages of the deposition, which levels off at a thickness of about 10 nm. At higher Ar pressures (0.5-6 Pa), $(F/w)_{int}$ increases almost linearly with film thickness up to 300 nm, where the deposition was stopped. The slope of the $(F/w)_{int}$ curve is highest at 0.5 Pa, similar to that previously observed by Klokholm and Berry.[11] Upon increasing the Ar pressure to 2 or 6 Pa, the slope of the force curve and, accordingly, the related stress decrease significantly. The stress dependence on sputter pressure is summarized in Fig. 2, which shows the average intrinsic stress calculated by Eq. (1) for the continuous Co films, i.e., at thicknesses above 10 nm. After the deposition the stress becomes immediately constant and does not change during the next 16 h, demonstrating that the stress relaxation is negligible in the entire range of sputter pressures investigated.

Figure 3 shows the cross-sectional FIB images of the Co films deposited at different sputter pressures. The FIB images clearly show that the Co films sputtered at higher sputter pressures (0.5, 2, and 6 Pa) grow by columnar grains. The average grain size decreases from about 80 to 60 nm with increasing sputter pressure.

The AFM investigation reveals that the surface roughness of the Co films increases considerably upon raising the sputter pressure. Two examples at sputter pressures of 0.05 and 6 Pa are shown in Figs. 4(a) and 4(c), respectively. Whereas at 0.05 Pa the roughness is as low as 0.5 nm, it increases by more than one order of magnitude to 6 nm for a sputter pressure of 6 Pa. The results obtained by the SEM [Figs. 4(b) and 4(d)] are similar to those obtained by the AFM investigations. Interestingly, for samples deposited at higher pressures (2 and 6 Pa) pronounced black contours separating the grains can be seen in the SEM images [Fig. 4(d)].This is the result of the "open" columnar microstructure.

We could not deduce the grain size from EBSD measure-

Downloaded 09 Feb 2006 to 193.174.238.119. Redistribution subject to AIP license or copyright, see http://jap.aip.org/jap/copyright.jsp

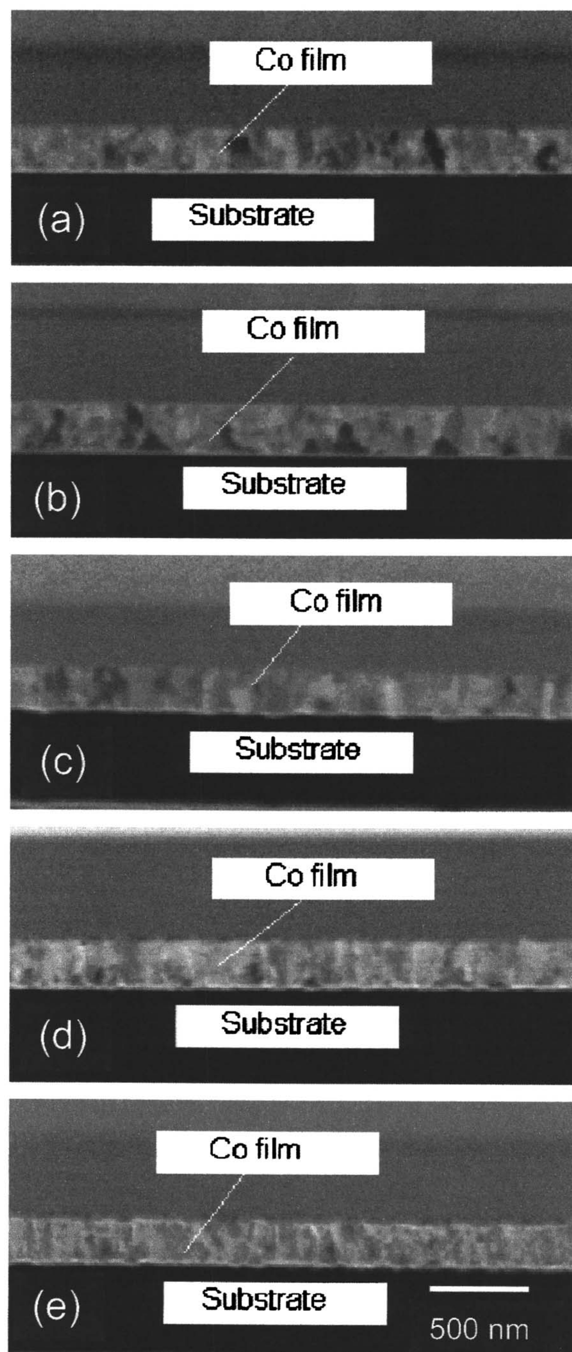

FIG. 3. The cross-sectional FIB images of Co films with a thickness of about 300 nm and deposited with a rate of 0.05 nm/s at Ar pressures of (a) 0.05 Pa, (b) 0.2 Pa, (c) 0.5 Pa, (d) 2 Pa, and (e) 6 Pa.

ments because no diffraction patterns were obtained which might be a hint for very small and/or distorted crystallites.

Also, the electrical resistance and the mass density of the Co films depend significantly on the sputter pressure. Whereas the resistance increases with sputter pressure, the mass density of the film decreases. The results of the microstructure investigations, mass density, and resistivity data are summarized in Table I.

IV. DISCUSSION

As revealed by our experiments, the stress, growth, and morphology of the sputtered Co films as well as their physical properties are characterized by a strong dependence on the sputter pressure. Our structural investigations show that the Co films grow by the Volmer-Weber mode. The SEM images of the samples deposited at low Ar pressures (not shown here) confirm discontinuous film morphology at thicknesses below 10 nm. The film stress actually is very similar to that of polycrystalline metal films that are at the transition between high and low adatom mobilities (Sec. I). In the coalescence stage a large tensile stress develops due to the formation of grain boundaries,[18–21] which levels off when the films become continuous at a thickness of about 10 nm. This is consistent with the stress behavior of the low-mobility metal films prepared in previous studies by evaporation.[10]

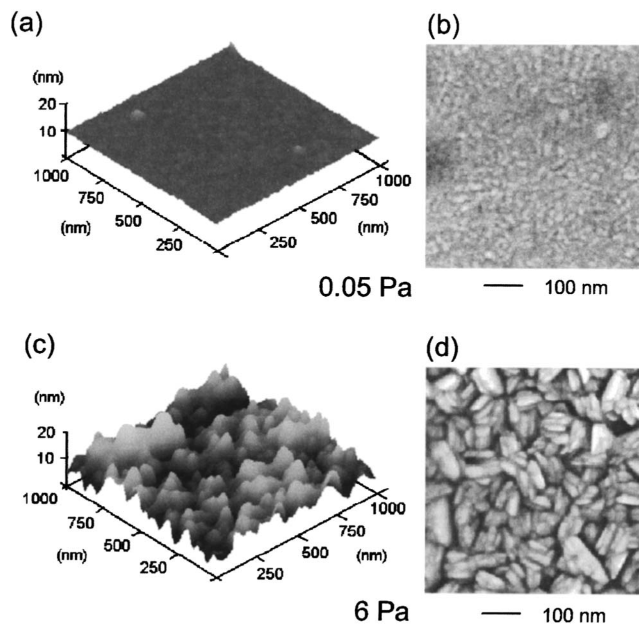

FIG. 4. The AFM [(a) and (c)] and SEM [(b) and (d)] images of 300-nm-thick Co films sputtered at Ar pressures of 0.05 and 6 Pa.

Beyond the initial stage of the deposition an inhomogeneous tensile stress is developed in the depth of Co films for all values of sputter pressure [Fig. 2(a)]. We assume that the microstructure which develops with film thickness has a dominant role for the development of the inhomogeneous stress in the film depth; i.e., for high sputter pressure, the open microstructure evolves with the increase of film thickness. The details of the stress dependence on the film thickness cannot be understood by the presented results. Therefore, further microstructure investigations are necessary in order to know how the microstructure evolves with film thickness.

Now we discuss the compressive stress contribution at low sputter pressures. Two mechanisms have been proposed in the literature for the compressive stress contribution appearing in the continuous films. For evaporated films capillarity effects[8] in the island stage were considered to generate a compressive strain field that is propagated into the continuous film upon further growth.[22] It decreases with film thickness when the strain information from the interface gets gradually lost due to incorporation of defects. For sputtered films the compressive stress has been attributed to lattice

Downloaded 09 Feb 2006 to 193.174.238.119. Redistribution subject to AIP license or copyright, see http://jap.aip.org/jap/copyright.jsp

TABLE I. The results of microstructure investigations, resistivity, and mass density data of Co films with a thickness of about 300 nm for various sputter pressures as indicated. Grain-size information has been obtained from FIB images by interactive linear analysis. The surface roughness is represented by a root-mean-square (rms) value determined over a 1×1 μm^2 area of the AFM images.

Sputter pressure	0.05 Pa	0.2 Pa	0.5 Pa	2 Pa	6 Pa
Grain size (nm) (FIB cut)	83		88		62
Surface roughness (rms) (nm)	0.5	0.8	2.0	3.6	6.0
Resistivity (10^{-8} Ωm) (Resistivity of bulk Co at RT is 5.7×10^{-8} Ωm.)	10.5	10.4	14.3	45.2	69.8
Mass density (10^3 kg/m^3) (Mass density of bulk Co at RT is 8.90×10^3 kg/m^3.)	5.84		5.60		4.75

distortions produced by energetic particles striking the film, a mechanism known as "atomic peening".[23,24] In the experiments presented here [Fig. 2(a)] and also for sputtered Cu films[16] the compressive stress contribution decreases again at a thickness of about 150 nm, a finding that is accounted for only by the first mechanism.

As evidenced by the FIB investigations, with increasing Ar pressure a transition to columnar grain growth takes place. This change in the grain growth has to be attributed to a decreasing kinetic energy of the Co atoms as a direct consequence of the increasing slowing down and thermalization of the sputtered particle flux in collisions with the sputter gas atoms. Again in agreement with previous studies[10,11] the stress of such films is tensile and dominated by the grain-boundary relaxation mechanism.[18] A linear increase of F/w with film thickness is expected, which is nearly fulfilled for the $(F/w)_{\text{int}}$ curve at 0.5 Pa.

At Ar pressures above 0.5 Pa the tensile stress decreases again. In a recent study by Misra and Nastasi[25] a similar behavior was observed for sputtered Cr films. The cross-sectional transmission electron microscopy on the Cr films prepared at higher sputter pressures ($>$0.5 Pa) revealed a columnar porosity at the grain boundaries. As discussed by Misra and Nastasi[25] and Muller[26] the density at the grain boundaries strongly affects the interatomic forces there and can explain the lowering of the tensile stress. Such a porous morphology is obtained when the kinetic energy of the impinging target atoms becomes too small due to the increasing thermalization at higher sputter pressures. In fact, our SEM investigations indicate a more open microstructure at the grain boundaries for the samples deposited at Ar pressures above 0.5 Pa, which, accordingly, is responsible for the observed reduction of the tensile stress.

The evolution from a relatively dense to a more open microstructure with higher surface roughness is further corroborated by the increase in electrical resistivity measured at RT from about 10×10^{-8} to 70×10^{-8} Ωm and by the reduction of the mass density from 5.84×10^3 to 4.75×10^3 kg/m^3.

V. CONCLUSIONS

We investigated the stress of sputtered Co films at various sputter pressures (0.05-6 Pa) up to a thickness of 300 nm and related it to the morphology. At low sputter pressures (0.05-0.2 Pa) the evolution of stress and morphology resembles that of Volmer-Weber metal films with medium adatom mobility. A large tensile stress due to grain-boundary formation dominates only in the discontinuous films. With increasing sputter pressure the kinetic energy of the sputtered Co atoms decreases due to rising collisions with the sputter gas phase and a transition to columnar grain growth takes place. Accordingly, a nearly constant tensile stress is observed during the entire growth, which reaches its maximum value at a sputter pressure of about 0.5 Pa. At even higher sputter pressures the microstructure of the Co films becomes more open, indicating that the surface mobility of the impinging atoms has decreased further and the tensile stress contribution is reduced again. The evolution of stress can be fully understood and described by a combination of the stress mechanisms proposed already in the literature for evaporated and sputtered films. The sputter pressure proves to be a sensitive deposition parameter for controlling the stress, growth, and morphology of sputtered thin films.

ACKNOWLEDGMENTS

The authors would like to thank T. Mühl for useful suggestions, M. Stangl for resistivity measurements, and I. Fiering, C. Krien, and R. Vogel for technical assistance. This work was supported by the Deutsche Forschungsgemeinschaft (Project No. SCHN 353/15-2).

[1] J. F. Liu, J. Y. Feng, and W. Z. Li, Nucl. Instrum. Methods Phys. Res. B **194**, 289 (2002).
[2] S. Parkin, X. Jiang, C. Kaiser, A. Panchula, K. Roche, and M. Samant, Proc. IEEE **91**, 661 (2003).
[3] J. F. Bobo, L. Gabillet, and M. Bibes, J. Phys.: Condens. Matter **16**, S471 (2004).
[4] A. Gerber, *et al.* J. Magn. Magn. Mater. **242**, 90 (2002).
[5] D. Elefant, D. Tietjen, R. Schaefer, D. Eckert, R. Kaltofen, M. Mertig, and C. M. Schneider, J. Appl. Phys. **91**, 8590 (2002).
[6] J. I. Hong, S. Sankar, A. E. Berkowitz, and W. F. Egelhoff, J. Magn. Magn. Mater. **285**, 359 (2005).
[7] R. Koch, D. Winau, A. Führmann, and K. H. Rieder, Phys. Rev. B **44**, 3369 (1991).
[8] R. Abermann, R. Kramer, and J. Mäser, Thin Solid Films **52**, 215 (1978).
[9] R. Abermann, Mater. Res. Soc. Symp. Proc. **239**, 25 (1992).
[10] R. Koch, J. Phys.: Condens. Matter **6**, 9519 (1994).
[11] E. Klokholm and B. S. Berry, J. Electrochem. Soc. **115**, 823 (1968).
[12] Th. Gutjahr-Löser, D. Sander, and J. Kirschner, J. Magn. Magn. Mater. **220**, L1 (2000).
[13] D. Sander, S. Ouazi, V. S. Stepanyuk, D. I. Bazhanov, and J. Kirschner, Surf. Sci. **512**, 281 (2002).
[14] Z. Zhou and Y. Fan, Thin Solid Films **272**, 43 (1996).
[15] J. A. Thornton, J. Tabock, and D. W. Hoffmann, Thin Solid Films **64**, 111 (1979).
[16] M. Pletea, W. Brückner, H. Wendrock, and R. Kaltofen, J. Appl. Phys. **97**, 054908 (2005).

Downloaded 09 Feb 2006 to 193.174.238.119. Redistribution subject to AIP license or copyright, see http://jap.aip.org/jap/copyright.jsp

[17]G. G. Stoney, Proc. R. Soc. London, Ser. A **82**, 172 (1909).
[18]F. A. Doljack and R. W. Hoffman, Thin Solid Films **12**, 71 (1972).
[19]W. D. Nix and B. M. Clemens, J. Mater. Res. **14**, 3467 (1999).
[20]S. C. Seel, C. V. Thompson, S. J. Hearne, and J. A. Floro, J. Appl. Phys. **88**, 7079 (2000).
[21]L. B. Freund and E. Chason, J. Appl. Phys. **89**, 4866 (2001).
[22]R. Abermann, R. Koch, and R. Kramer, Thin Solid Films **58**, 365 (1979).
[23]F. M. d'Heurle, Metall. Trans. **1**, 725 (1970).
[24]H. J. Windischmann, J. Vac. Sci. Technol. A **9**, 2431 (1991).
[25]A. Misra and M. Nastasi, J. Mater. Res. **14**, 4466 (1999).
[26]K.-H. Müller, Phys. Rev. B **35**, 7906 (1987).

Downloaded 09 Feb 2006 to 193.174.238.119. Redistribution subject to AIP license or copyright, see http://jap.aip.org/jap/copyright.jsp